Robust Interacting Particle-Kalman Filter based structural damage estimation using dynamic strain measurements under non-stationary excitation -an experimental study

Neha Aswal, Eshwar Kuncham, Subhamoy Sen, Laurent Mevel

Robust Interacting Particle-Kalman Filter based structural damage estimation using dynamic strain measurements under non-stationary excitation - an experimental study

Neha Aswal[1], Eshwar Kuncham[1], Subhamoy Sen[1], Laurent Mevel[2]
[1] School of Engineering, Indian Institute of Technology Mandi, 175005 Mandi, India
[2] Univ. Gustave Eiffel, Inria, COSYS-SII, I4S Team, 35042 Rennes, France
email: nehaaswal96@gmail.com, eshwar.research@gmail.com, subhamoy@iitmandi.ac.in, laurent.mevel@inria.fr

ABSTRACT: Sensor types and their positioning is a major factor in structural health monitoring (SHM) to ensure certainty in estimation. While acceleration has predominantly been employed for damage detection, they are known to be costly and not frame invariant (except for moderately accurate GPS based accelerometers). A thorough monitoring of a real life structure requires dense instrumentation which might become expensive with costly sensor types. Further, damages mostly occur at rare events, like seismic base excitation, for which typical accelerometers are not proper. This study employs strain as a cheaper alternative for damage sensitive measurement that is also frame invariant. An interacting filtering approach with particle and Kalman filters is employed that estimates structural health from measured dynamic strains. Further to account for extreme non-stationary events like seismic excitation, robustness against uncertain inputs is induced in the filtering environment following an output injection approach. The proposed algorithm is tested on a seven story-one bay frame model and a real experimental beam structure.

KEY WORDS: Structural Health Monitoring; Interacting Filters; Particle Filter; Kalman Filter; Damage Detection.

1 INTRODUCTION

The objective of this paper is to monitor structures, subjected to non-stationary input forces through the response measurements, recorded using a network of sensors. To ascertain safety in structures, damages due to strong forces or extreme service conditions should be detected immediately after their occurrence. Traditionally, structural health monitoring (SHM) research employs deterministic approaches for real time structural damage detection with no consideration about the uncertainties originating from unavoidable model inaccuracies, sensor noises and unknown external disturbances [1–3]. This limits the utility of the methods for real field applications. Bayesian filtering technique has been proved to be an efficient alternative that can promptly detect anomaly in structures in the presence of such uncertainties [4–8].

Efficiency of SHM approaches depends on the density and positioning of the measurement locations. Nevertheless, cost of sensors and the accessibility of the location where the sensors are supposed to be placed pose the major challenge in real life application. In reality, following the financial constraints, the measured data are often sparse compromising the precision in system health estimation. However, employing a suitably selected numerical model (typically Finite Element Models (FEM)), the auxiliary correlation information between these sparse and non-collocated measured data, obtained from the conceptual models, can additionally be incorporated [8]. While this model-based approach benefits by reducing the estimation uncertainty obvious for sparse dataset, it demands a precise numerical model.

The involvement of a numerical model in estimation inherently introduces modelling uncertainty besides the uncertainty due to measurement noises. Bayesian filtering based techniques can simultaneously handle model and measurement uncertainties. Structural health is further parameterized in this attempt and subsequently estimated typically employing acceleration as measurement. Yet, the acceleration sensors are costly and their placement on the nodes (structural joints) are not always easy due to the accessibility reasons. Also, under the base excitation conditions, the accelerometer fails to provide a reference independent response as measurement. Due to these practical complexities involved with acceleration sensors, frame invariant and comparatively cheaper strain gauges can be considered as an alternative for real life SHM problems. However, this demands a numerical model to map the system states to corresponding strain measurement.

Also, for filtering-based SHM approaches typical assumption on stationarity and/or Gaussianity for ambient forcing does not hold true for extreme loading conditions, like, earthquakes or high wind/waves. Eventually, with a forced idealization about the input, the algorithms may perform poorly for forcing scenarios that are not Gaussian and stationary. Present study discusses one such possibility in which the structural damage is required to be estimated under non-stationary forcing. To induce robustness against input forcing, current study takes basis of [9]'s work in which an output injection approach is adopted in order to reject the input. The system estimation is performed using an interacting filtering strategy in which a Kalman filter estimates the system states while a Particle

filter monitors the variation in health parameters.

Further, since this study adopts strain as measurement, a model is required to map system states (typically displacement and velocity) to corresponding strain. The strain-displacement relationship is therefore developed through an FEM approach taking basis on the shape functions. The proposal is validated on a seven story-one bay frame structure involving 21 members and 84 *degrees-of-freedom*(*dof*). Further, real experiments are performed on a cantilever beam to calibrate its material properties and detect the presence of damage in the beam.

2 STATE SPACE FORMULATION FOR THE SYSTEM DYNAMICS

The governing differential equation for a typical linear time varying (LTV) mechanical system with $(n \times n)$ order mass, stiffness and damping matrices being $\mathbf{M}$, $\mathbf{K}$ and $\mathbf{C}$ (n is number of *dof*) can be represented as,

$$\mathbf{M}(t)\ddot{\mathbf{q}}(t) + \mathbf{C}(t)\dot{\mathbf{q}}(t) + \mathbf{K}(t)\mathbf{q}(t) = \mathbf{f}(t) - \mathbf{M}(t)\tau\ddot{\mathbf{a}}^g(t) \quad (1)$$

$\ddot{\mathbf{q}}(t)$, $\dot{\mathbf{q}}(t)$ and $\mathbf{q}(t)$ are the system's acceleration, velocity and displacement responses, respectively. $\mathbf{f}(t)$ is the external ambient force acting on the structure. $\ddot{\mathbf{a}}^g(t)$ is the ground acceleration (as disturbance input) and τ is the location matrix that maps the effect of ground excitation to each of the nodes of the system. With $\mathbf{F}(t) = \begin{bmatrix} \mathbf{0}_n & \mathbf{I}_n \\ -\mathbf{M}(t)^{-1}\mathbf{K}(t) & -\mathbf{M}(t)^{-1}\mathbf{C}(t) \end{bmatrix}_{2n\times 2n}$, $\mathbf{B}_c(t) = \begin{bmatrix} \mathbf{0}_n \\ \mathbf{M}(t)^{-1} \end{bmatrix}_{2n\times m}$, $\mathbf{E}_c = \begin{bmatrix} \mathbf{0} \\ \tau \end{bmatrix}_{2n\times l}$ and $\mathbf{x}(t) = \begin{bmatrix} \mathbf{q}^T(t) & \dot{\mathbf{q}}^T(t) \end{bmatrix}^T_{2n\times 1}$, the system dynamics, given in Equation (1), can be described in its continuous time as

$$\dot{\mathbf{x}}(t) = \mathbf{F}(t)\mathbf{x}(t) + \mathbf{B}_c(t)\mathbf{u}(t) + \mathbf{E}_c\ddot{\mathbf{a}}_g(t) + \mathbf{v}(t) \quad (2)$$

where $\mathbf{x}(t)$ denotes the unobserved system state. $\mathbf{0}_n$ and $\mathbf{I}_n$ are the n^{th} order null and identity matrices respectively. $\mathbf{u}(t)_{m\times 1}$, being the ambient forcing on the structure, can be modeled as a stationary white Gaussian noise (SWGN) of constant covariance $\mathbf{Q}_{m\times m}$. $\mathbf{v}(t)$ is the process noise modeled as SWGN with covariance $\mathbf{Q}^v_{2n\times 2n}$. However, no SWGN model can be defined for $\ddot{\mathbf{a}}^g_{l\times 1}$. l is the number of channels for the disturbance input. The discrete time representation of the system is as follows,

$$\mathbf{x}_k = \mathbf{F}_k\mathbf{x}_{k-1} + \mathbf{B}_k\mathbf{u}_k + \mathbf{E}_k\ddot{\mathbf{a}}^g_k + \mathbf{v}_k \quad (3)$$

with $\mathbf{F}_k$, $\mathbf{B}_k$, $\mathbf{E}_k$, $\mathbf{x}_k$, $\mathbf{u}_k$, $\mathbf{x}_k$, $\mathbf{v}_k$ and $\ddot{\mathbf{a}}^g_k$ correspond to their continuous time entities described earlier obtained through zero-order-hold technique. The system's unobserved states are estimated using dynamic strain as measurement with the measurement equation defined as,

$$\varepsilon_k = \mathbf{H}_k\mathbf{x}_k + \mathbf{w}_k \quad (4)$$

where, $\mathbf{H}_{kp\times 2n}$ is the time dependent measurement function that maps the system states $\mathbf{x}_k$ to the corresponding strain measurements $\varepsilon_{kp\times 1}$. In reality, $\mathbf{H}_k$ signifies the strain displacement relationship modeled using the finite element approach for all the members combined. This mapping takes basis on Equation (26) (Appendix) and combines for all measured members. $\mathbf{w}_{kp\times 1}$ denotes the measurement noise originating from the sensors and can be modeled as an SWGN of constant covariance $\mathbf{R}_{p\times p}$.

3 SYSTEM ESTIMATION WITH ROBUST INTERACTING PARTICLE-KALMAN FILTER

This article proposes an interacting strategy (also called as Rao-Blackwellisation [10–12, 8, 13, 7]) combining a Particle Filter (PF) with a Kalman Filter (KF), similar to IPKF algorithm given by [6], which further improvises the state filter with induced robustness through output injection following [9], discussed later. Overall, the approach employs a PF in which particles represent the posterior distribution of the health parameters as a numerical approximation, while KF deals with the uncertainty in the state space. PF being robust to nonlinear systems have been employed for parameter estimation while KF estimates the system states since a linear system is considered in this study [14]. Prior to demonstrate the proposed IPKF algorithm, the involved robustness aspect has been discussed in the following.

3.1 Robust Kalman filter

Typical KF requires either the exactly known inputs or an idealized SWGN model of it. For seismic excitation, none of these idealizations is valid which calls for induction of robustness within the KF algorithm [15–18]. A previously developed method [7] achieves the robustness against unknown input forces by estimating the forces in real-time through an additional force filter. Yet, this additional computation makes the algorithm slow and less prompt from the damage detection perspective. The study employs [9]'s robust approach that rejects the impact of the unknown input $\ddot{\mathbf{a}}^g_k$ in the state evolution by suitably injecting a part of the measured output in the state transition model. Owing to the measurement equation (cf. Equation (4)), the following holds true for an arbitrary bounded matrix $\mathbf{G}_k \in \mathbb{R}^{2n\times m}$,

$$0 = \mathbf{G}_k\left(\mathbf{y}_k - \mathbf{H}_k\mathbf{x}_k - \mathbf{w}_k\right) \quad (5)$$

Adding Equation (3) with Equation (5) and further setting $\mathcal{L}_k = \mathbf{I}_{2n} - \mathbf{G}_k\mathbf{H}_k$, the state equation, Equation (3), can be modified as

$$\begin{aligned} \mathbf{x}_k &= \mathbf{F}_k\mathbf{x}_{k-1} + \mathbf{B}_k\mathbf{u}_k + \mathbf{E}_k\ddot{\mathbf{a}}^g_k + \mathbf{v}_k + \\ &\quad \mathbf{G}_k\left(\mathbf{y}_k - \mathbf{H}_k\mathbf{x}_k - \mathbf{w}_k\right) \\ &= \tilde{F}_k\mathbf{x}_{k-1} + \tilde{B}_k\mathbf{u}_k + \tilde{E}_k\ddot{\mathbf{a}}^g_k + \mathbf{G}_k\mathbf{y}_k + \tilde{\mathbf{v}}_k \end{aligned} \quad (6)$$

with $\tilde{F}_k = \mathcal{L}_k\mathbf{F}_k$, $\tilde{B}_k = \mathcal{L}_k\mathbf{B}_k$, $\tilde{E}_k = \mathcal{L}_k\mathbf{E}_k$ and $\tilde{\mathbf{v}}_k = \mathbf{v}_k - \mathbf{G}_k\mathbf{w}_k$. If $\mathbf{G}_k$ is chosen such that $\mathbf{G}_k = \mathbf{E}_k(\mathbf{H}_k\mathbf{E}_k)^\dagger$, with † denoting Moore-Penrose Pseudo-inverse operation, $\tilde{E}_k$ renders to a null matrix. Equation (6) can then be

transformed to Equation (7), decoupled from the unknown input $\ddot{\mathbf{a}}_k^g$ as

$$\mathbf{x}_k = \tilde{F}_k \mathbf{x}_{k-1} + \tilde{B}_k \mathbf{u}_k + \mathbf{G}_k \mathbf{y}_k + \tilde{\mathbf{v}}_k \tag{7}$$

Again $\tilde{\mathbf{v}}_k$ can be idealized as an SWGN process. By this new formalism, Equation (3) has been transformed to Equation (7) in order to reject the unknown input $\ddot{\mathbf{a}}_k^g$ with an appropriate injection of the known output $\mathbf{y}_k$. Equation (4) can still be used as the associated measurement equation. With this approach, the state filter can be employed without any explicit or statistical knowledge of the unknown input forces due to ground acceleration $\ddot{\mathbf{a}}_k^g$.

3.2 PF-based parameter estimation

PF attempts system uncertainty propagation through a cloud of N_p independent parameter particles $\Xi_k = [\xi^1, \xi^2, \cdots, \xi^N]$ and their evolution [19, 20]. At any arbitrary time step k, the evolution of an arbitrary particle ξ_{k-1}^i is basically a random perturbation around its current position,

$$\xi_k^j = \xi_{k-1}^j + \mathbb{N}(\delta\xi_k, \sigma_k^\xi) \tag{8}$$

where a Gaussian blurring is performed on ξ_{k-1}^j with a shift $\delta\xi_k$ and a spread of σ_k^ξ [1]. The perturbed positions for the particles are then re-centered for consistency. This re-centring is actually a second step evolution in which particles are pushed towards the particle mean. For this, the same evolution strategy is adopted, as has been adopted in [7]. The evolved particles are subsequently weighted based on their likelihood against the current measurement to find the posterior.

3.3 Nested KF-based state estimation

Inside the KF, state is estimated for each of the j^{th} particle. The estimation propagates current estimation ($\mathbf{x}_{k-1|k-1}^j$), conditioned on the current parameter estimate for each j^{th} particle, to the predicted value, $\mathbf{x}_{k|k-1}^j$ following Equation (9),

$$\mathbf{x}_{k|k-1}^j = \tilde{F}_k^j \mathbf{x}_{k-1|k-1}^j + \mathbf{G}_k^j \mathbf{y}_k \tag{9}$$

with corresponding state covariance, $\mathbf{P}_{k|k-1}^j$,

$$\mathbf{P}_{k|k-1}^j = \tilde{F}_k^j \mathbf{P}_{k-1|k-1}^j \tilde{F}_k^{jT} + \tilde{B}_k^j \mathbf{Q}_k \tilde{B}_k^{jT} + \mathbf{G}_k^j \mathbf{R}_k \mathbf{G}_k^{jT} \tag{10}$$

with $\mathbf{Q}_k$ and $\mathbf{R}_k$ being covariances of process and measurement noise.

The corresponding measurement predictions $\mathbf{y}_{k|k-1}^{i,j}$ can be obtained exploiting Equation (4). Associated innovation, $\epsilon_{k|k-1}^j$, can be obtained through estimating the departure of prediction from the real measurement $\mathbf{y}_k$. Next, Kalman gain, $\mathbf{K}_k^j$, is calculated as,

$$\mathbf{K}_k^j = \frac{\mathbf{P}_{k|k-1}^j \mathbf{H}_k^T}{\mathbf{H}_k \mathbf{P}_{k|k-1}^j \mathbf{H}_k^T + \mathbf{R}_k} \tag{11}$$

The predicted states and state covariance are updated accordingly,

$$\mathbf{x}_{k|k}^j = \mathbf{x}_{k|k-1}^j + \mathbf{K}_k^j \epsilon_{k|k-1}^j \tag{12}$$

$$\mathbf{P}_{k|k}^j = (\mathbf{I} - \mathbf{K}_k^j \mathbf{H}_k) \mathbf{P}_{k|k-1}^j \tag{13}$$

3.4 Particle approximation

Likelihood of each particle, i.e. $\mathcal{L}(\xi_k^j)$, is further calculated based on the innovation mean $\epsilon_{k|k-1}^j$ and co-variance, $\mathbf{S}_k^j$, of each KF. The normalized weight for each j^{th} particle is further updated as,

$$w(\xi_k^j) = \frac{w(\xi_{k-1}^j)\mathcal{L}(\xi_k^j)}{\sum_{j=1}^N w(\xi_{k-1}^j)\mathcal{L}(\xi_k^j)} \tag{14}$$

with $\mathcal{L}(\xi_k^j) = \left((2\pi)^n \sqrt{|\mathbf{S}_k|}\right)^{-1} e^{-0.5 \bar{\epsilon}^{jT} \mathbf{S}_k{}^{-1} \bar{\epsilon}^j}$. The particle approximations for the parameters and states are then estimated as:

$$\mathbf{x}_{k|k} = \sum_{j=1}^N w(\xi_k^j) \mathbf{x}_{k|k}^j; \quad \text{and} \quad \theta_{k|k} = \sum_{j=1}^N w(\xi_k^j) \xi_k^j \tag{15}$$

4 NUMERICAL EXPERIMENT

The numerical investigation is performed with an FE model of a two dimensional seven-storey one-bay shear frame (cf. Figure 1) considered as the "test structure" for the experimentation (as a proxy for the real concrete structure). The relevant material and geometric details are presented in Table 1. The model is defined with six noded (three translational and three rotational) Euler Bernoulli beam elements. A 2% Rayleigh damping is further assumed for damping.

The structure is excited at its base using north-south component of El-centro earthquake (Data source: `http://peer.berkeley.edu/research/motions/`). Synthetic strain responses are further simulated from this model under ambient as well as base excitation in its healthy as well as damaged condition. The sampling frequency, time series length, time of arrival of seismic excitation, and time of damage occurrence has been maintained constantly at 50 Hz, 1024, 2 seconds and 3 seconds, respectively. The sensors are assumed to be patched onto the soffit of beam members only. Dynamic strain measurements collected from the members have been considered as response data which is further contaminated with stationary white Gaussian noise (SWGN) of *signal-to-noise-ratio* (*snr*) 1% to replicate real life scenario.

It is obvious that with increasing size of particle pool, the estimation accuracy and precision is supposed to be

[1] $A + B\mathbb{N}(\mu, \sigma)$ means $A + Bz$ where z follows $\mathbb{N}(\mu, \sigma)$

Table 1: Geometry and material properties of the frame

Beam section dimension	$0.2m \times 0.3m$
Column section dimension	$0.3m \times 0.3m$
Elasticity	$3 \times 10^{12} Pa$
Density	$2500 kg/m^3$

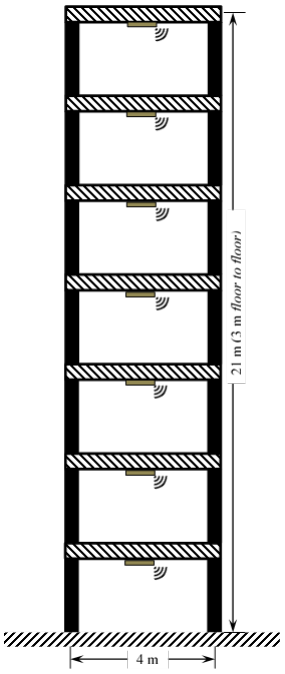

Figure 1: Schematic diagram of the experimental frame structure

enhanced. Yet, this comes at an enhanced computational cost as well, which ideally should be maintained at a manageable limit. The numerical experiment employed 3000 particle for PF.

Figure 2 presents the adopted north-south component of the seismic ground motion time history taken from the El-Centro ground motion data. In parallel, the comparison between estimated strains against measured strains is also demonstrated. The strain estimation is done through reproducing the member strains from estimated states. It can be verified from Figure 2, that even after introduction of the non-stationary base excitation, the proposed algorithm perfectly estimated the strains as well as detected damage location and intensity with accuracy and precision. The real time damage detection is presented in Figure 3, where from the promptness and accuracy of detection can be verified.

5 EXPERIMENTAL STUDY - CANTILEVER BEAM

The proposed algorithm has been experimentally tested on an aluminium cantilever beam with material and geometric specifications shown in Table 2.

The beam is segmented into 4 elements with a focus to estimate health indices (***hi***s) for each of the segments. The first three elements of the beam starting from the fixed support are instrumented with strain gauges (Gauge

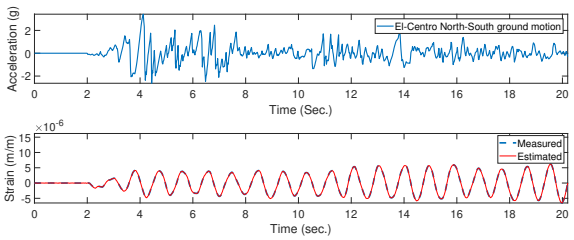

Figure 2: Reproduced strain from the estimated states

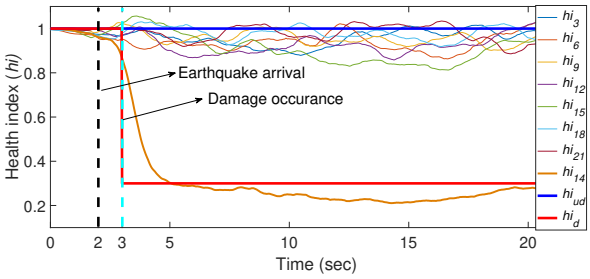

Figure 3: Real time damage detection: Numerical study

Table 2: Properties of cantilever beam

Cross section	$22mm \times 6mm$
Length	$400mm$
Density	$2700 kg/m^3$
Calibrated elasticity	$65.5e9 Pa$

length 5 mm and resistance 350 Ω) in full bridge configuration placed on the centre of the corresponding elements (denoted here as e_1, e_2, and e_3). An additional accelerometer is also attached to the tip of the beam to obtain frequency response function (FRF) for model calibration purpose (cf. Figure 4). Both the accelerometer and the strain gauges are sampled at a fixed sampling rate of 2000 Hz for very long time (30 sec). The cantilever beam is subjected to arbitrary as well as known input forces through an impact hammer. The known input force later facilitates in obtaining the FRF for the beam set up, required for model calibration.

Next, a primary finite element model for the undamaged experimental beam set up is created using Euler Bernoulli beam element with assumed material properties, which is later calibrated using the FRF obtained from modal domain decomposition of the measured accelerations with Fast Fourier Transform (FFT). This first phase of calibration was done manually targeting to bring the primary model sufficiently close to the reality. For this, initial material elasticity is adopted from tensile testings previously performed on the same material. This elasticity value is then uniformly altered for all the elements to arrive close to the experimentally obtained FRF.

Simultaneously, FFT of the strain gauge signals has been performed to cross-check the working of the assembled full-bridge strain gauges. Signals obtained from accelerometer and strain gauges led to the same experimental frequency

(first two frequencies: $\omega_1 = 27.34$ Hz and $\omega_2 = 187.40$ Hz) of the undamaged cantilever beam which also ascertained the reliability of the full-bridge assembly.

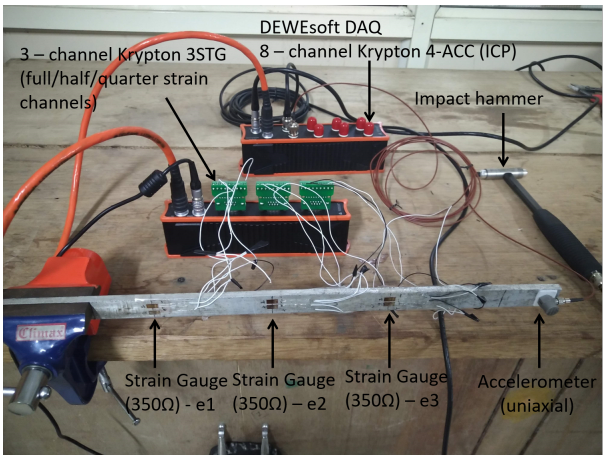

Figure 4: Experimental set up

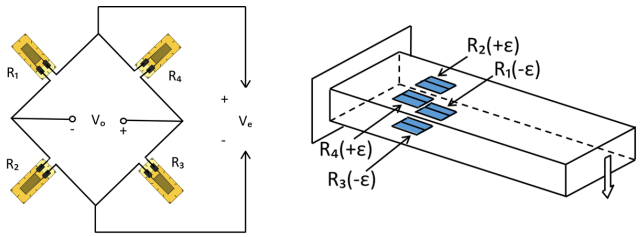

Figure 5: Full-bridge strain gauge configuration

The manually calibrated model is then employed as the undamaged predictor model with the proposed r-IPKF algorithm along with the strain gauge measurements obtained from the undamaged structure to further calibrate the element elasticity in accordance to the experimental conditions. A set of four ***hi***s has been defined within a range of 0 to 100% that gets multiplied with the assumed elasticity values in the primary model. These ***hi***s are then estimated using the proposed algorithm as parameter states. Thus the health of the element can also be tracked using such ***hi***s assuming 0 and 100 % denoting complete failure and healthy state of the element, respectively. 500 particles have been selected for PF with $\alpha = 0.98$ while the initial distribution for each ***hi*** is considered as Gaussian, $\mathcal{N}(1, 0.01)$. The estimated ***hi***s are presented in Figure 6 where minute calibrations can be observed to be implemented on element level elasticity. Once calibrated, the updated predictor model perfectly replicates the reality.

Next, damage is induced in the cantilever by removing a volume of $7 \times 22 \times 3mm^3$ from the $e2$ element of the beam as shown in the schematic diagram (cf. Figure 7). The signals (cf. Figure 8) obtained from the strain gauges patched on the elements, $e1 - e3$, are then run through the r-IPKF. Figure 10, histograms of the input strain signals for the algorithm, demonstrates the non-stationary nature of the input forcing. The strain signals have a sampling rate of 100 Hz with a time series length of 2048. The

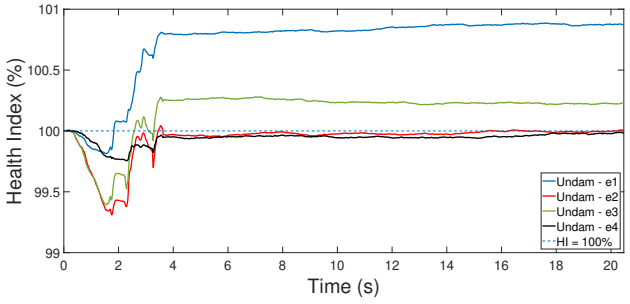

Figure 6: Model calibration with undamaged response

result, thus obtained, shows a drop in pre-calibrated ***hi*** to ***hi*** $= 83.5\%$ for the second element, which corresponds roughly to a 16.5% damage in that element (cf. Figure 9) when compared to the initial rigidity value.

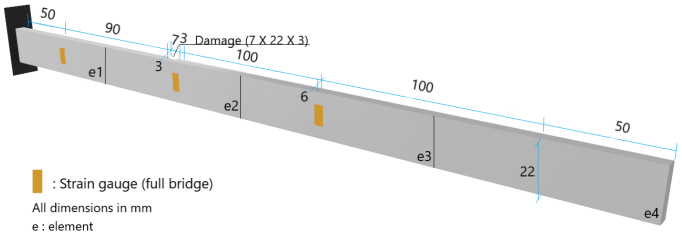

Figure 7: Schematic model of the damaged cantilever beam

6 CONCLUSION

This article demonstrates an interacting filtering-based SHM algorithm that is robust against arbitrary forcing. The proposed method couples a particle filter for health parameter estimation with Kalman filter that estimates the system states from the measured noisy response data. The robustness against arbitrary input forcing in induced within the state filter following an output injection technique given by [9]. Strain has been adopted in this study for the measurement due to their cheaper installation cost and frame invariant nature. The proposed method has been validated using simulated strain response data from a numerical frame structure as well as on a real cantilever beam structure. While for the numerical experiment, non-stationary seismic base excitation has been employed as force, for the experiment, it has been ensured that the input forcing is not stationary or Gaussian. Both validation study establishes the promptness, robustness and efficacy of the proposed algorithm.

REFERENCES

[1] Charles R Farrar, TA Duffy, Phillip J Cornwell, and Scott W Doebling. Excitation methods for bridge structures. Technical report, Los Alamos National Lab., NM (US), 1999.

[2] Peter Cawley and Robert Darius Adams. The location of defects in structures from measurements of natural frequencies. *The Journal of Strain Analysis for Engineering Design*, 14(2):49–57, 1979.

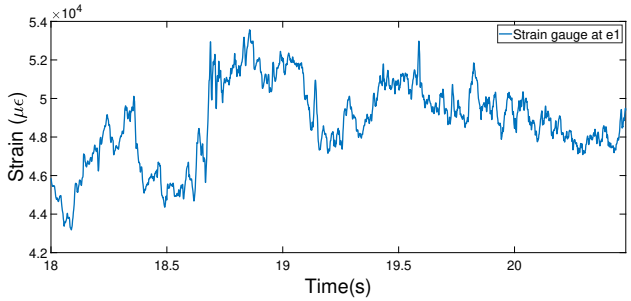

(a) Measured strain response at first sensor point

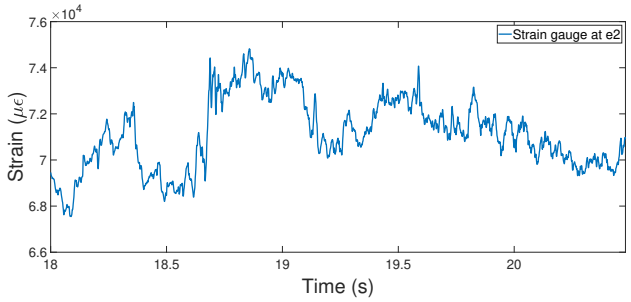

(b) Measured strain response at second sensor point

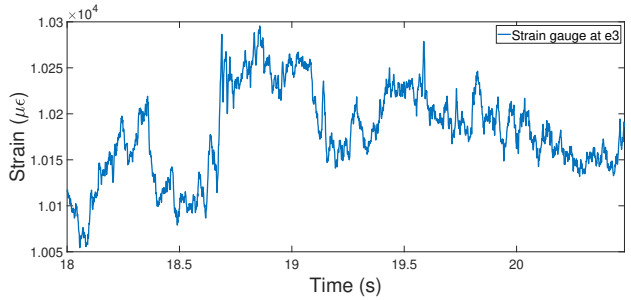

(c) Measured strain response at third sensor point

Figure 8: Measured strain response of the damaged cantilever beam

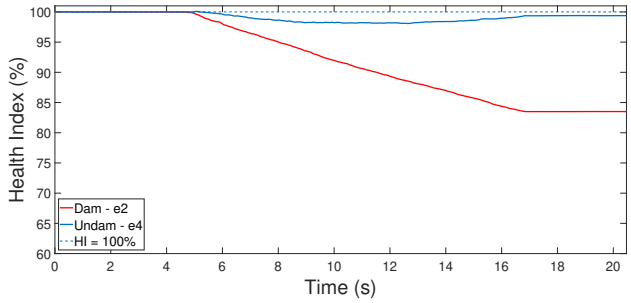

Figure 9: Real time damage detection: Experimental study

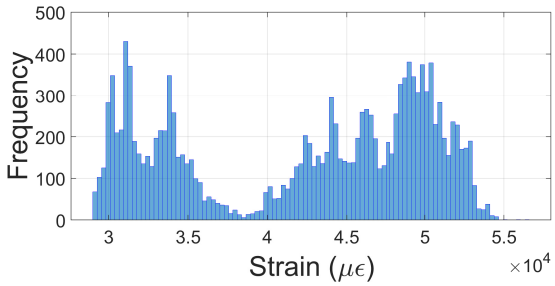

(a) Histogram of measured strain response at first sensor point

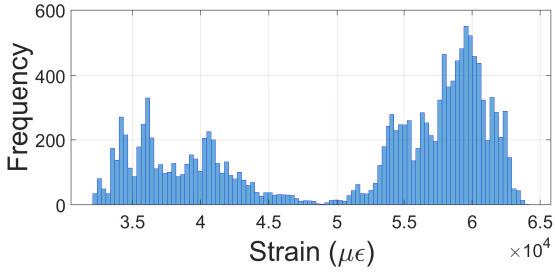

(b) Histogram of measured strain response at second sensor point

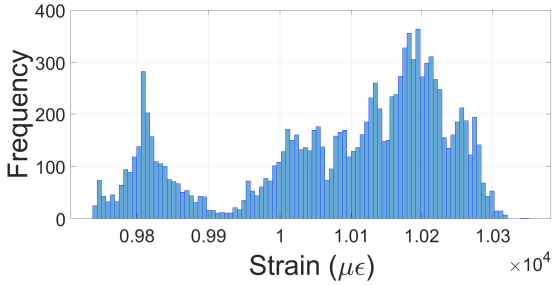

(c) Histogram of measured strain response at third sensor point

Figure 10: Histogram of measured strain response of the damaged cantilever beam

[3] Y_ Narkis. Identification of crack location in vibrating simply supported beams. *Journal of sound and vibration*, 172(4):549–558, 1994.

[4] Guillaume Mercère, Laurent Bako, and Stéphane Lecœuche. Propagator-based methods for recursive subspace model identification. *Signal Processing*, 88(3):468–491, 2008.

[5] Laurent Mevel, Albert Benveniste, Michèle Basseville, Maurice Goursat, Bart Peeters, Herman Van der Auweraer, and Antonio Vecchio. Input/output versus output-only data processing for structural identification—application to in-flight data analysis. *Journal of Sound and Vibration*, 295(3-5):531–552, 2006.

[6] Meriem Zghal, Laurent Mevel, and Pierre Del Moral. Modal parameter estimation using interacting kalman filter. *Mechanical Systems and Signal Processing*, 47(1-2):139–150, 2014.

[7] Subhamoy Sen, Antoine Crinière, Laurent Mevel, Frédéric Cérou, and Jean Dumoulin. Seismic-induced damage detection through parallel force and parameter estimation using an improved interacting particle-kalman filter. *Mechanical Systems and Signal Processing*, 110:231–247, 2018.

[8] Subhamoy Sen and Baidurya Bhattacharya. Online structural damage identification technique using constrained dual extended kalman filter. *Structural Control and Health Monitoring*, 24(9):e1961, 2017.

[9] Qinghua Zhang and Liangquan Zhang. State estimation for stochastic time varying systems with disturbance rejection. *IFAC-PapersOnLine*, 51(15):55–59, 2018.

[10] Arnaud Doucet, Nando De Freitas, Kevin Murphy, and Stuart Russell. Rao-blackwellised particle filtering for dynamic bayesian networks. In *Proceedings of the Sixteenth conference on Uncertainty in artificial intelligence*, pages 176–183. Morgan Kaufmann Publishers Inc., 2000.

[11] Pierre Del Moral and Feynman-Kac Formulae. Genealogical and interacting particle systems with applications. probability and its applications, 2004.

[12] Subhamoy Sen and Baidurya Bhattacharya. Progressive damage identification using dual extended kalman filter. *Acta Me-*

chanica, 227(8):2099–2109, 2016.
[13] Saeed Eftekhar Azam, Aldo Ghisi, and Stefano Mariani. Parallelized sigma-point kalman filtering for structural dynamics. *Computers & Structures*, 92:193–205, 2012.
[14] Anneke Hommels, Akira Murakami, and Shin-Ichi Nishimura. A comparison of the ensemble kalman filter with the unscented kalman filter: application to the construction of a road embankment. *Geotechniek*, 13(1):52, 2009.
[15] Peter K Kitanidis. Unbiased minimum-variance linear state estimation. *Automatica*, 23(6):775–778, 1987.
[16] Steven Gillijns and Bart De Moor. Unbiased minimum-variance input and state estimation for linear discrete-time systems with direct feedthrough. *Automatica*, 43(5):934–937, 2007.
[17] E Lourens, Costas Papadimitriou, Steven Gillijns, Edwin Reynders, Guido De Roeck, and Geert Lombaert. Joint input-response estimation for structural systems based on reduced-order models and vibration data from a limited number of sensors. *Mechanical Systems and Signal Processing*, 29:310–327, 2012.
[18] Ming Ge and Eric C. Kerrigan. Noise covariance estimation for time-varying and nonlinear systems. *IFAC Proceedings Volumes*, 47(3):9545 – 9550, 2014. ISSN 1474-6670. 19th IFAC World Congress.
[19] Eleni N Chatzi and Andrew W Smyth. The unscented kalman filter and particle filter methods for nonlinear structural system identification with non-collocated heterogeneous sensing. *Structural Control and Health Monitoring*, 16(1):99–123, 2009.
[20] S Eftekhar Azam, M Bagherinia, and Stefano Mariani. Stochastic system identification via particle and sigma-point kalman filtering. *Scientia Iranica*, 19(4):982–991, 2012.

7 APPENDIX: STRAIN-DISPLACEMENT RELATION

With strain as measurement, a measurement model is required to map the states to corresponding strains. The system dynamics defined in equation 1 has been solved using FEM approach and the nodal displacement values are obtained. With a strain-displacement relationship defined using the associated shape functions, strains at members can be obtained through interpolation. In the following, the pertinent strain-displacement relation for a frame structure is detailed.

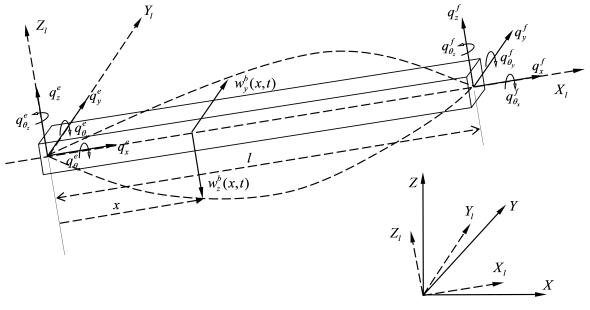

Figure 11: Assumed Euler-Bernoulli Beam element with local and global degrees of freedom

3D Euler-Bernoulli beam has been considered as the elements for the FEM solution of the frame structure. Relevant schematic is presented in Figure 11. For each element, two transverse displacements, $w_y(x,t)$ and $w_z(x,t)$, are the field variables which can be interpolated at any arbitrary point x along the length of the beam (cf. Figure 11) using the nodal displacements and the associated shape functions. Further, deflection of a frame member at any direction can be idealized as summations of deflection due to its beam action and truss action, as:

$$\begin{aligned} w_y(x,t) &= w_y^b(x,t) + w_x^t(x,t) \\ w_z(x,t) &= w_z^b(x,t) + w_x^t(x,t) \end{aligned} \tag{16}$$

The deflection transverse to the beam orientation due to beam, i.e., $w^b(x,t)$, action at any arbitrary distance x can be interpolated using the nodal displacements $q^l(t)$ defined in local coordinate system as:

$$w^b(x,t) = \begin{bmatrix} w_y^b(x,t) \\ w_z^b(x,t) \end{bmatrix} = \psi^b(x) q^l(t) \tag{17}$$

where, $\psi^b(x)$ is the interpolation matrix that transforms nodal displacements $q^l(t)$ to corresponding transverse displacements. $q^l(t)$ can further be retrieved from the nodal displacements defined in global degrees of freedom through coordinate transformation as:

$$q^l(t) = \mathbf{T}\mathbf{q}(t) \tag{18}$$

where $\mathbf{T}$ is the coordinate transformation matrix. $\psi^b(x)$ is constituted with the interpolation functions as:

$$\psi^b(x) = \begin{bmatrix} 0 & \psi_1(x) & 0 & 0 & 0 & \psi_2(x) & \cdots \\ 0 & 0 & \psi_1(x) & 0 & \psi_2(x) & 0 & \cdots \\ \cdots & 0 & \psi_3(x) & 0 & 0 & 0 & \psi_4(x) \\ \cdots & 0 & 0 & \psi_3(x) & 0 & \psi_4(x) & 0 \end{bmatrix} \tag{19}$$

where,

$$\begin{aligned} \psi_1(x) &= \frac{1}{4}(1-\eta)^2(2+\eta); \quad \psi_2(x) = \frac{L}{8}(1-\eta)^2(1+\eta) \\ \psi_3(x) &= \frac{1}{4}(1+\eta)^2(2-\eta); \quad \psi_4(x) = \frac{L}{8}(1+\eta)^2(\eta-1) \end{aligned} \tag{20}$$

with $\eta = 2x/L - 1$ and, nodal displacement $q^l(t)$ can be expanded as:

$$q^l(t) = \begin{bmatrix} q_x^e & q_y^e & q_z^e & q_{\theta_x}^e & q_{\theta_y}^e & q_{\theta_z}^e & \cdots \\ \cdots & q_x^f & q_y^f & q_z^f & q_{\theta_x}^f & q_{\theta_y}^f & q_{\theta_z}^f \end{bmatrix}^T \tag{21}$$

Similarly, slope and curvature at any arbitrary point x can be calculated as:

$$\begin{aligned} \theta^b(x) &= w^b(x,t)' = \psi^{b'}(x) q^l(t) \\ \kappa^b(x) &= \frac{(1+\theta^b(x,t)^2)^{\frac{3}{2}}}{w^{b''}(x,t)} \end{aligned} \tag{22}$$

where,

$$w^{b''}(x,t) = \psi^b(x)'' q^l(t) \tag{23}$$

The curvature is further measured in the form of longitudinal strain (ε^{xx}) using a strain gauge patched at the surface of the beam. This gauge will register total strain due to both beam action and truss action. The strain due

to bending in the beam is obtained from this curvature equation as:

$$\varepsilon^{xx,b}(x,t) = -y_0/\kappa^b(x,t) \tag{24}$$

where y_0 is the distance of extreme fiber from the neutral axis where the strain gauge is patched. The strain due to truss action can also be obtained as:

$$\varepsilon^{xx,t}(x,t) = -\frac{1}{l}(q_x^e - q_x^f) \tag{25}$$

where l is the length of the element. The total strain can further be obtained as:

$$\varepsilon^{xx}(x,t) = \varepsilon^{xx,b}(x,t) + \varepsilon^{xx,t}(x,t) \tag{26}$$